Neutron stars with hyperon cores

Author: Glòria Montaña Faiget
Facultat de Física, Universitat de Barcelona, Diagonal 645, 08028 Barcelona, Spain.

Advisor: Àngels Ramos Gómez

Abstract: The composition and structure of neutron stars are studied employing different models for the equation of state of neutron star matter allowing for the appearance of hyperons. The models are constructed with simple but realistic parametrizations of the nucleon-nucleon and hyperon-nucleon interactions. Solving the equations of hydrostatic equilibrium it is found that there is only one model able to predict a maximum neutron star mass over $2\,M_\odot$, in agreement with astronomical observations. This is a model which has a soft nucleonic contribution to the energy density but a stiff hyperonic one and, as a consequence, avoids the hyperonization of matter.

I. INTRODUCTION

Neutron stars are the ultradense compact remnants of massive stars [1]. These objects are an exceptional laboratory to test our understanding of nuclear matter because they have supranuclear interior densities that can reach as high as 10 times the saturation density $\rho_0 = 0.16\,\mathrm{fm}^{-3}$ (the density of nucleon matter in heavy atomic nuclei). Their internal structure can be divided in regions of different physical properties and composition, as shown in Fig. 1, and depends on the equation of state (EOS), i.e. the pressure and energy density dependences on the baryon density, $P(\rho_B)$ and $\varepsilon(\rho_B)$.

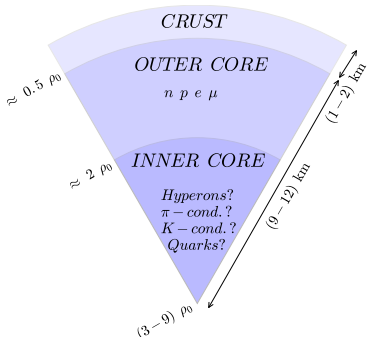

FIG. 1: Schematic illustration of the internal structure of a neutron star.

The properties of finite nuclei constrain the EOS at $\rho \leq \rho_0$. In contrast, the high densities of the inner core are not yet possible to be produced in laboratories and thus the detailed composition of neutron star cores is still unknown. Several hypothesis are being considered, such as the appearance of hyperons, pion and kaon condensations or a phase transition to deconfined quark matter. Since the EOSs are very model dependent, astro-observational data is, for the moment, the only mechanism capable to rule out the inaccurate models.

The present work is focused on the study of the influence of hyperons in the composition and structure of neutron stars. Hyperons, which are baryons containing at least one strange quark, are unstable on Earth and decay to nucleons through weak interactions. However, the formation of hyperons is possible at increasing nucleon densities. Neutron stars are mainly supported against their own gravitation by the degeneracy pressure of fermions. Assuming $T = 0$, the pressure is given by the Fermi seas of the constituent particles. Due to the Pauli exclusion principle, at high densities it is more energetically favourable to have a hyperon than a nucleon and thus the hyperonization of matter leads to the relieve of the Fermi pressure, i.e. to the *softening* of the EOS.

Models of neutron star EOSs can be classified into *stiff* (or *hard*) and *soft* regarding to the compressibility of matter. The EOS determines the mass-radius relationship and the corresponding maximum neutron star mass. The soft hyperonized models yield low maximum masses ($\sim 1.4\,M_\odot$). The recent discovery of massive neutron stars ($\sim 2\,M_\odot$) [2, 3] supports stiffest EOSs and supposes an obstacle for the models with hyperon cores, yet hyperons seem to be unavoidably present in neutron stars [4].

II. FORMALISM

A. β-equilibrium composition

In the following description we consider the matter in neutron star cores composed of a mixture of N_B baryons (B) and N_l leptons (l) in β-equilibrium. This requires chemical equilibrium of weak processes of the type

$$B_1 \longrightarrow B_2 + l + \bar{\nu}_l \quad ; \quad B_2 + l \longrightarrow B_1 + \nu_l \tag{1}$$

$$l_1 \longrightarrow l_2 + \nu_{l_1} + \bar{\nu}_{l_2}. \tag{2}$$

Further constraints are obtained by demanding charge neutrality and baryon number conservation

$$\sum_i \rho_{B_i} = \rho_B \tag{3}$$

$$\sum_i q_{B_i}\rho_{B_i} + \sum_j q_{l_j}\rho_{l_j} = 0, \tag{4}$$

where ρ_{B_i} and ρ_{l_j} are the partial densities of each baryon and lepton species respectively, ρ_B is the total baryon density, q_{B_i} are the electric charges of the baryons and q_{l_j} the ones for leptons.

At densities around ρ_0, matter is composed of neutrons, protons and electrons. Once the rest mass of the muon is exceeded by the electron chemical potential, muons can be formed by $e^- \longrightarrow \mu^- + \nu_e + \bar{\nu}_\mu$. Larger densities permit the appearance of hyperonic degrees of freedom. For instance, when the neutron chemical potential exceeds the threshold energy for the appearance of a Λ (i.e., its interaction energy with the nucleons added to its rest mass), it is more energetically favourable for a neutron at the top of its Fermi sea to decay to a Λ. This may happen at densities above $2-3\,\rho_0$.

At baryon densities $\rho_B \lesssim 10\,\rho_0$, significant for neutron star cores, it is enough to consider the octet of lightest baryons, including the nucleon doublet N, the singlet Λ, the triplet Σ and the doublet Ξ. Previous works on this topic [5, 6] reflect that the Λ and the negatively charged Σ^- and Ξ^- are the most probable appearing hyperons in neutron stars. Thus for the sake of simplicity, we take into account matter composed of $np\Lambda\Sigma^-\Xi^- e^-\mu^-$, for which the equilibrium relations can be summarized in

$$\begin{gathered}\mu_\Lambda = \mu_n = \mu_p + \mu_e\,, \quad \mu_\Sigma = \mu_\Xi = \mu_n + \mu_e\,, \quad \mu_\mu = \mu_e \\ \rho_n + \rho_p + \rho_\Lambda + \rho_\Sigma + \rho_\Xi = \rho_B \\ \rho_p = \rho_\Sigma + \rho_\Xi + \rho_e + \rho_\mu. \end{gathered} \tag{5}$$

Note that these equations ignore μ_{ν_l} and $\mu_{\bar{\nu_l}}$ because the neutrino mean free path is larger than the typical radius of neutron stars. Therefore, neutron star matter can be assumed transparent to ν_l and $\bar{\nu}_l$.

Since the chemical potentials are related to the EOS through $\mu_i = \partial\varepsilon\{\rho_j\}/\partial\rho_i$, we have $\mu_i = \mu_i\,(\{\rho_j\})$ and Eqs. (5) constitute a system of seven nonlinear equations that determine, for each value of the baryon density ρ_B, the densities $\{\rho_j\}$ of the seven species in β-stable neutron star matter. In this piece of work, the roots are numerically solved using the globally convergent Newton routine *newt* described in [7].

The β-equilibrium compositions $\{\rho_j\}$ enable the determination of $\varepsilon(\{\rho_j\})$ and $P(\{\rho_j\})$ that constitute the EOS of the β-equilibrated star matter. For the subnuclear densities in the crust, the EOS of BPS Negele [8] is used.

B. TOV equations

The next step in the formalism is to calculate the neutron star properties predicted by the EOSs to test their validity.

For a given EOS, $P = P(\rho_B)$, the mass and radius of a star with a central density ρ_{B_C} can be determined by numerical integration of the Tolman-Oppenheimer-Volkoff equations (TOV) [9, 10] of hydrostatic equilibrium for non-rotating compact objects

$$\frac{dm}{dr} = 4\pi r^2 \rho_B(r)$$

$$\begin{aligned}\frac{dP}{dr} = -G\frac{m(r)\rho_B(r)}{r^2}\left(1+\frac{P(r)}{\rho_B(r)}\right)\left(1+4\pi r^3\frac{P(r)}{m(r)}\right)\cdot \\ \cdot\left[1-\frac{2Gm(r)}{r}\right]^{-1}, \end{aligned} \tag{6}$$

where the terms in brackets account for relativistic corrections to the Newtonian equations.

These equations are solved by setting a central density ρ_{B_C} and integrating outwards by Euler's method (with a small enough integration step) until reaching zero pressure. This produces the relationships $M(\rho_{B_C})$ and $R(\rho_{B_C})$ and yields the prediction of a neutron star maximum mass for each EOS.

III. MODELS

The internal energy of neutron star matter at $T = 0$ may be divided into a baryon part, which includes kinetic, potential and mass contributions, and a lepton part, which only has kinetic and mass terms since leptons are treated as non-interacting particles:

$$\begin{aligned}\varepsilon_{\rm tot} = \varepsilon_{\rm kin}(\{\rho_{B_i}\}) + \varepsilon_{\rm pot}(\{\rho_{B_i}\}) + \varepsilon_{\rm mass}(\{\rho_{B_i}\}) \\ + \varepsilon_{\rm kin}(\{\rho_{l_j}\}) + \varepsilon_{\rm mass}(\{\rho_{l_j}\}).\end{aligned} \tag{7}$$

The contributions to the pressure are easily derived from the total energy density:

$$\begin{aligned}P &= \sum_i \rho_{B_i}\mu_{B_i} + \sum_j \rho_{l_j}\mu_{l_j} - \varepsilon_{\rm tot} \\ &= \sum_i \rho_{B_i}\frac{\partial\varepsilon_{\rm tot}\{\rho_k\}}{\partial\rho_{B_i}} + \sum_j \rho_{l_j}\mu_{l_j} - \varepsilon_{\rm tot}.\end{aligned} \tag{8}$$

The non-relativistic kinetic energy density of the baryons at $T = 0$ is given by

$$\varepsilon_{\rm kin}\left(\{\rho_{B_i}\}\right) = \sum_i \frac{\hbar^2}{2m_{B_i}}\frac{3}{5}\left(3\pi^2\right)^{2/3}\rho_{B_i}^{5/3}, \tag{9}$$

and the contribution to the energy density of the baryonic mass is

$$\varepsilon_{\rm mass}\left(\{\rho_{B_i}\}\right) = \sum_i \rho_{B_i} m_{B_i}, \tag{10}$$

where m_{B_i} is the mass of the baryon species i.

The leptons are treated relativistically and their contributions read

$$\begin{aligned}&\varepsilon_{\rm kin}(\{\rho_{l_j}\}) + \varepsilon_{\rm mass}(\{\rho_{l_j}\}) = \\ &\sum_j \frac{1}{8\pi}\left[2k_{\rm F}\mu_{l_j}^3 - k_{\rm F}m_{l_j}^2\mu_{l_j} - m_{l_j}^4\ln\frac{k_{\rm F}+\mu_{l_j}}{m_{l_j}}\right],\end{aligned} \tag{11}$$

where the lepton chemical potential and Fermi momentum are given by

$$\mu_{l_i} = \sqrt{m_{l_i}^2 + k_{\rm F}^2}\,, \quad k_{\rm F} = (3\pi^2\rho_{l_i})^{1/3}. \tag{12}$$

For the potential energy density term, we use a series of simple but realistic parametrizations that must

reproduce the baryon interactions to the better possible extent. However, the limitation of the experimental data and the lack of knowledge of the strong interactions at supranuclear densities make it possible to explore different models and test different choices of the parameters.

For the pure nucleonic contribution two distinct interaction models are considered. The first one is an analytic parametrization of the nucleonic energy per baryon developed by Heiselberg and Hjorth-Jensen [11] and includes the kinetic term besides the nuclear interactions,

$$e(\rho_N, x_p) = e_0 u \frac{u-2-\delta}{1+u\delta} + s_0 u^\gamma (1-2x_p)^2, \qquad (13)$$

where $u = \rho/\rho_0$, $x_p = \rho_p/\rho_N$, and $\rho_N = \rho_n + \rho_p$ is the nucleon density. Then, the contribution to the energy density is

$$\varepsilon^{\mathrm{HH}}_{\mathrm{pot},N} + \varepsilon^{\mathrm{HH}}_{\mathrm{kin},N} = e(\rho_N, x_p)\rho_N. \qquad (14)$$

The values of the parameters are displayed in Table I.

e_0 (MeV)	s_0 (MeV)	γ	δ
15.8	32	0.6	0.2 / (0.15)

TABLE I: Values of the parameters corresponding to the nucleonic EOS of the HH model, Eq. (13).

The second model for the nucleonic contribution to $\varepsilon_{\mathrm{pot}}$ is an approach by Balberg and Gal [5] and consists of an attractive term, a term yielding isospin dependence and a third repulsive term

$$\varepsilon^{\mathrm{BG}}_{\mathrm{pot},N}(\rho_n, \rho_p) = \frac{1}{2}\left[a_{NN}\rho_N^2 + b_{NN}(\rho_n - \rho_p)^2 + c_{NN}\rho_N^{\delta+1}\right]. \qquad (15)$$

Table II displays the parameters for the nuclear model derived in [5].

δ	a_{NN} (MeV fm^3)	b_{NN} (MeV fm^3)	c_{NN} (MeV fm$^{3\delta}$)
5/3	−935.4	214.2	1557.2

TABLE II: Values of the parameters corresponding to the nucleon interaction energy density in the BG model, Eq. (15).

An easy test that can support these models is the comparison with experimental data of heavy ion collisions (HIC) [12]. Figure 2 depicts the nucleonic EOSs of both symmetric matter and neutron matter.

Notice that the BG parametrization is considerably stiffer than the HH model at supranuclear densities. Only the soft HH EOS is compatible with the symmetric matter and the neutron matter experimental bands. Nonetheless, the stiff BG EOS passes through the edge of the allowed region in neutron matter, and, since neutron stars are mainly composed by neutrons, we consider this EOS as an example of the maximum acceptable nuclear stiffness.

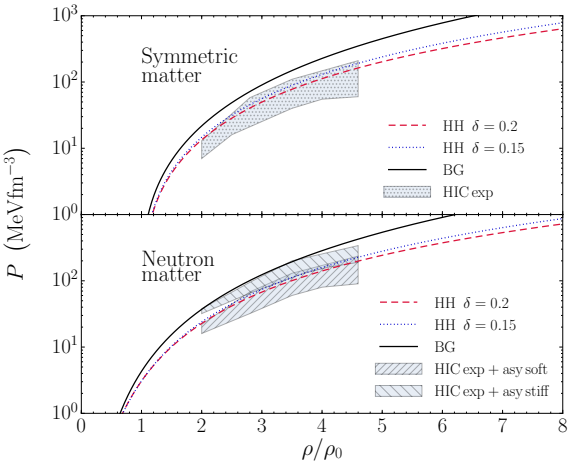

FIG. 2: Comparison of the EOS given by the models with the heavy ion collisions experimental data of symmetric matter and neutron matter.

For the hyperon interaction potential the BG parametrization is used again, although only YN interactions are taken into account. The experimental data regarding YY is considerably scarce and because nucleons are the main constituents of matter in most of the density range, NN and YN interactions dominate over the YY ones. The corresponding potential energy density is

$$\begin{aligned}\varepsilon^{\mathrm{BG}}_{\mathrm{pot},YN}(\{\rho_{x_i}\}) = {} & a_{\Lambda N}\rho_N\rho_\Lambda \\ & + c_{\Lambda N}\left(\frac{\rho_N}{\rho_N+\rho_\Lambda}\rho_N^\gamma\rho_\Lambda + \frac{\rho_\Lambda}{\rho_N+\rho_\Lambda}\rho_\Lambda^\gamma\rho_N\right) \\ & + a_{\Sigma N}\rho_\Sigma\rho_N + b_{\Sigma N}(\rho_n-\rho_p)\rho_\Sigma \\ & + c_{\Sigma N}\left(\frac{\rho_N}{\rho_N+\rho_\Sigma}\rho_N^\gamma\rho_\Sigma + \frac{\rho_\Sigma}{\rho_N+\rho_\Sigma}\rho_\Sigma^\gamma\rho_N\right) \\ & + a_{\Xi N}\rho_\Xi\rho_N + b_{\Xi N}(\rho_n-\rho_p)\rho_\Xi \\ & + c_{\Xi N}\left(\frac{\rho_N}{\rho_N+\rho_\Xi}\rho_N^\gamma\rho_\Xi + \frac{\rho_\Xi}{\rho_N+\rho_\Xi}\rho_\Xi^\gamma\rho_N\right)\end{aligned} \qquad (16)$$

Hyperonic interactions are fixed by single particle potentials in nuclear matter at saturation density ρ_0. Experimental data reflect that Λ hypernuclei are well described by a potential depth of the Λ at ρ_0 of about -30 MeV. The situation for the rest of hyperons is far less clear. The Σ potential depth is fairly sure repulsive, while there is experimental evidence that the Ξ potential is attractive, although significantly less than that for the Λ. In our model we take $V_\Lambda(\rho_N = \rho_0) = -28$ MeV as in [5] and fix $V_\Sigma(\rho_N = \rho_0) = +30$ MeV and $V_\Xi(\rho_N = \rho_0) = -15$ MeV [13]. The unconstrained behaviour at high densities allows the choice of different parametrizations depending on the stiffness, determined by γ (see Table III).

Figure 3 depicts the density dependence of the hyperonic potentials for the parametrizations considered in Table III. Notice that $\gamma = 4/3$ corresponds to the softest potentials, while $\gamma = 2$ produces rather stiff potentials.

	γ	a_{YN} (Mev fm^3)	b_{YN} (Mev fm^3)	c_{YN} (Mev fm$^{3\gamma}$)
Λ	4/3	−505.2	-	605.5
	5/3	−387.0	-	738.8
	2	−340.0	-	1087.5
Σ	4/3	−130	214.2	602
	5/3	−15	214.2	723
	2	40	214.2	990
Ξ	4/3	−376	0	520.1
	5/3	−288	0	663.4
	2	−241	0	932.5

TABLE III: Values of the parameters corresponding to the hyperonic contribution in the BG model, Eq. (16).

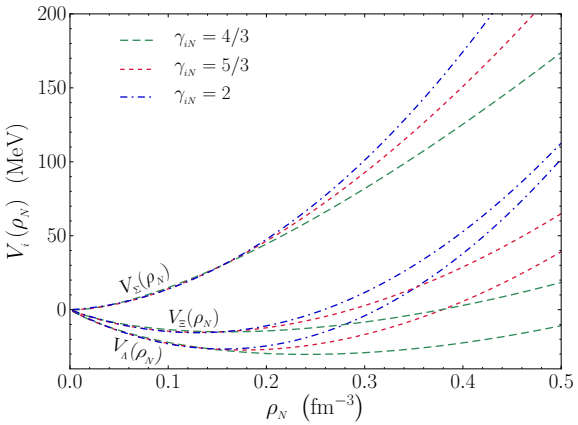

FIG. 3: Λ, Σ and Ξ potentials as a function of the density in symmetric nuclear matter, $V_i = a_{iN}\rho_N + c_{iN}\rho_N^{\gamma_{iN}}$.

In [5], Balberg and Gal examine the values $\delta = \gamma = \frac{4}{3}, \frac{5}{3}, 2$, changing simultaneously the stiffness of the nucleonic and hyperonic parts of $\varepsilon_{\rm pot}$. We here fix the stiffness of the nucleonic potential and then explore the various hyperonic stiffnesses varying the parameter γ. This results in six different models. The ones referred to as HHBG consist of the Heiselberg&Hjorth-Jensen nucleonic part and the Balberg&Gal hyperonic contribution. The ones indicated with BG take both contributions from Balberg&Gal parametrization, with the nucleonic part set to $\delta = \frac{5}{3}$. In view of the results obtained, an extra HHBG model is considered, with $\delta = 0.15$ for the nucleonic part and $\gamma = 2$ for the hyperonic one.

IV. RESULTS

The models above yield the composition of β-stable matter displayed in Fig. 4 up to $\rho_B = 1.5\,\text{fm}^{-3}$. The most remarkable feature is that hyperons appear at a density which varies from 0.3 to 0.5 fm^{-3}. The first hyperon species to appear is the Λ, closely followed by the Ξ^-. The Σ^- appears at higher densities due to the repulsive potential assumed for this species and it is even excluded in some models.

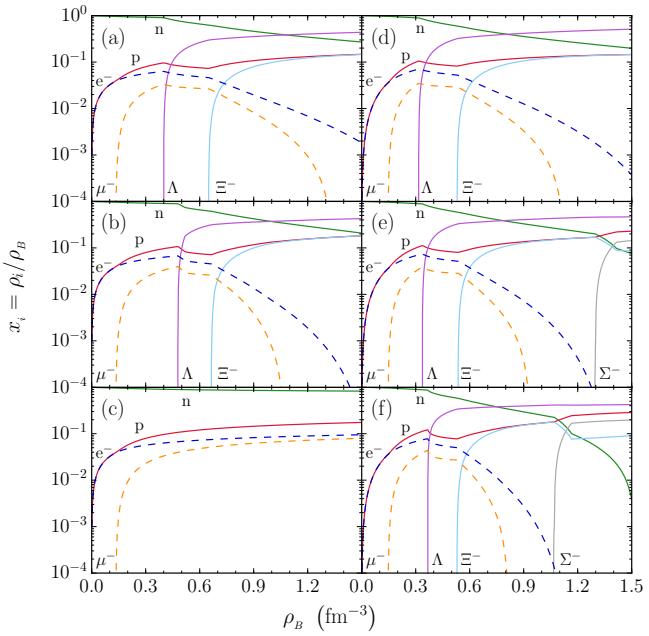

FIG. 4: β-equilibrium composition of neutron star matter. The panels on the left correspond to the HHBG models and the ones on the right to the BG models. Hyperonic stiffness increases from top to bottom with $\gamma = 4/3$ for (a) and (d), $\gamma = 5/3$ for (b) and (e) and $\gamma = 2$ for (c) and (f).

In the analysis of Fig. 4 one may notice that hyperonization happens somewhat earlier in the BG models than in the HHBG models. This can be understood in the way that the BG models have a stiffer nucleonic part. Also, hyperons appear at lower densities when hyperon interaction potentials are soft. Hyperon appearance is the reaction of the system to lower the energy density when the nucleonic potential is mildly attractive, or even repulsive, and thus it is favoured by both a stiff nucleonic model or a soft hyperonic model. For the same reason, when the contrary happens, the hyperonization of matter is disfavoured. Notice that in Fig. 4 (c) hyperons do not appear. Even if we stiffen the nucleonic part (HHBG model) by setting $\delta = 0.15$, still reproducing the HIC data as seen in Fig. 2, hyperons do not appear either.

It is also important to point out the deleptonization that follows hyperon appearance and which is specially powerful when the Ξ^- comes up. At low densities, leptons are needed to maintain charge neutrality, but as density is increased negatively charged hyperons offer an energetically cheaper option to maintain this condition.

The EOS of β-equilibrated matter are depicted in Fig. 5. We can clearly see that the models in which hyperons are present are characterized by a softening of the EOS with respect to those in which hyperons are naturally excluded.

The mass-radius relationships [14] obtained by solving the TOV equations are shown in Fig. 6. The EOSs of neutron star matter containing hyperons reach a maxi-

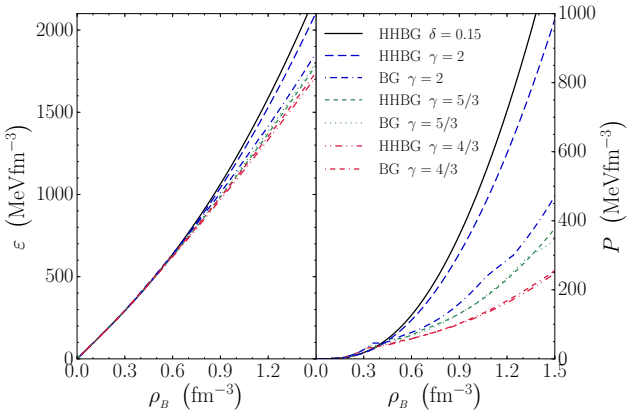

FIG. 5: Energy density ε and pressure P as a function of the baryonic density ρ_B for neutron star matter for the models under consideration.

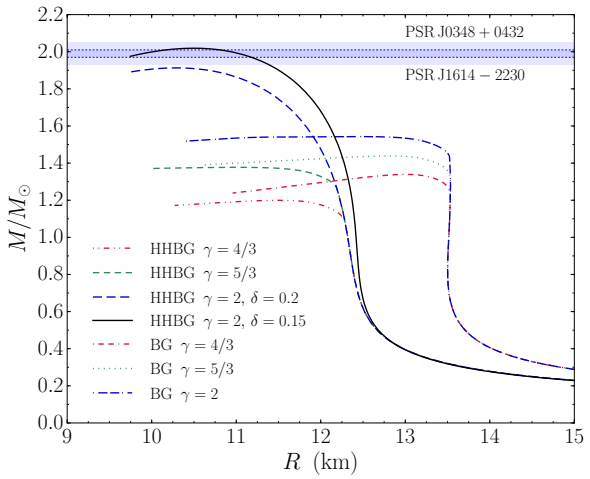

FIG. 6: Mass-radius relationship for different equations of state. Horizontal bands at $\approx 2\,M\odot$ are the observed masses of pulsars PSR J1614 − 2230 and PSR J0348 + 0432.

mum mass of $1.54\,M_\odot$, while that corresponding to the model that avoids the appearance of hyperons rises up to a value of $1.91\,M_\odot$. This prediction is almost compatible with the measurements of the large mass values of the pulsars PSR J1614 − 2230 ($1.97 \pm 0.04\,M_\odot$) [2] and PSR J0348 + 0432 ($2.01 \pm 0.04\,M_\odot$) [3]. It results that when making the nucleonic part of the HHBG model with $\gamma = 2$ somewhat stiffer ($\delta = 0.15$), the compatibility is achieved. This is similar to what was found recently in [15] with an *ab initio* quantum Monte Carlo calculation.

V. CONCLUSIONS

Employing simple parametrizations of the baryon-baryon interaction potentials, we have developed various models of β-stable neutron star matter including hyperonic degrees of freedom.

The appearance of hyperons leads to an inevitably softening of the EOS and a consequent reduction of the predicted maximum mass. YY interactions have not been considered but several authors report that the effect to the mass is only mild. Considering rotation of the star would also be insufficient to reach measured pulsar masses. Altogether it seems very difficult to find a model with hyperons yielding a stiff EOS.

What is relevant of our results is that we found a model for which the nucleonic EOS is soft enough and the hyperonic contribution is sufficiently stiff for hyperons being inherently excluded. If hyperons are actually not present in neutron star cores, stiff β-stable EOSs can be developed and high values of the maximum mass result.

Acknowledgments

I am deeply grateful to my advisor Àngels Ramos for guiding me throughout this project, for her remarks and suggestions as well as her patience and kindness. I also want to thank her for introducing me to nuclear physics research.

Thanks also to my family and friends for their support all over these years.

[1] Haensel, P., Potekhin, A. Y. & Yakovlev, D. G., *Neutron Stars 1: Equation of State and Structure*, (Springer Science+Business Media, LLC, New York, 2006).
[2] Demorest, P. B. et al., Nature (London) **467**, 1081 (2010).
[3] Antoniadis, J., Freire, P. C. C., Wex, N., et al., Science **340**, 448 (2013).
[4] Chatterjee, D., & Vidaña, I., Eur. Phys. J. A **52**, 29 (2016).
[5] Balberg, S., & Gal, A., Nucl. Phys. A **625**, 435 (1997).
[6] Đapo, H., Schaefer, B.-J., & Wambach, J. , Phys. Rev. C , **81**, 035803 (2010).
[7] Press, William H. et al. *Numerical Recipes in Fortran 77. The Art of Scientific Computing*, Chapter 9, Section 9.7, (Cambridge University Press, New York, 1997, 2nd ed.).
[8] Negele, J. W. & Vautherin D., Nucl. Phys. A **207**, 298 (1973).
[9] Oppenheimer, J. R., & Volkoff, G. M., Phys. Rev. **55**, 374 (1939).
[10] Tolman, R. C., Proc. Nat. Acad. Sci. USA **20**, 169 (1934).
[11] Heiselberg, H., & Hjorth-Jensen, M., Phys. Rep. **328**, 237 (2000).
[12] Danielewicz, P., Lacey, R., & Lynch, W. G., Science **298**, 1592 (2002).
[13] Gal, A., Hungerford, E. V., & Millener, D. J., Rev. Mod. Phys., in press, (2016). arXiv:1605.00557
[14] Ozel, F., & Freire, P., Annu. Rev. Astron. Astrophys., in press, (2016). arXiv:1603.02698
[15] Lonardoni, D., Lovato, A., Gandolfi, S., & Pederiva, F., Phys. Rev. Lett. **114**, 092301 (2015).